Images of Excited H_3^+ at the Foot of the Io Flux Tube in Jupiter's Atmosphere

J. E. P. Connerney, R. Baron, T. Satoh, T. Owen

The electrodynamic interaction between Io and the Jovian magnetosphere drives currents to and from the planet's ionosphere, where H_3^+ emission is excited. Direct images of this phenomenon were obtained with the ProtoCAM infrared camera at the National Aeronautics and Space Administration's 3-m Infrared Telescope Facility. The emissions are localized to the instantaneous foot of the Io flux tube, ≈8° equatorward of the more intense auroral H_3^+ emission associated with higher magnetic latitudes. The foot of the Io flux tube leads that of (undisturbed) model magnetic field lines passing through Io by 15° to 20° in longitude and is less visible in the northern hemisphere at longitudes where the surface magnetic field strength is greatest. These data favor the unipolar inductor model of the Io interaction and provide insight into the source location and generation of Jovian decameter radio emission.

Radio emission from the Jovian magnetosphere was first detected in 1955 (*1*) and has been monitored ever since by terrestrial observers and spacecraft (*2*). In 1964, Bigg discovered that the observation of high-frequency radio emission (22 MHz) was strongly correlated with the location of the satellite Io in its orbit about Jupiter (*3*). The probability of observation of Jovian decametric radio emission (DAM) at Earth is greatly increased when Io's orbital phase is near 90° or 240° (measured in the direction of Io's orbital motion from geocentric superior conjunction) and Io's magnetic latitude is large. This surprising result motivated much theoretical work on the interaction of Io with the Jovian magnetosphere and many observational studies germane to Io's influence on the Jovian magnetosphere.

Io orbits Jupiter at a radial distance of 5.9 R_J, where R_J is the radius of Jupiter, with an orbital period of 42.5 hours, whereas Jupiter and its magnetosphere rotate with a period of just under 10 hours. Io's motion relative to the corotating magnetospheric plasma ($\mathbf{v}$ = 57 km/s) results in a motional electric field $\mathbf{E} = \mathbf{v} \times \mathbf{B}$ in a frame of reference moving with Io that is canceled by the polarization electric field maintained by the conducting surface (ionosphere) of Io. In the unipolar inductor models (*4, 5*), this polarization electric field drives a current through a circuit that closes through the Jovian ionosphere at the foot of Io's flux tube (at both Jovian poles). The Io flux tube (IFT) consists of the Jovian magnetic field lines that intersect the equatorial plane within an Io radius (1820 km) of the satellite's instantaneous orbital position. In this model, the current is conducted along the entire length of the IFT between Io and Jupiter's ionosphere, leading to a significant displacement (in the direction of Io's orbital motion) of the IFT with respect to the undisturbed magnetic field. More recent models (*6*) conduct this charge away from Io in the form of an Alfvén wave launched nearly along the magnetic field direction toward the ionosphere. The Alfvén disturbance is confined to "wings" that make an angle θ with the magnetic field, where $\tan(\theta) = v/v_a$, v is the velocity of Io, and v_a is the Alfvén velocity of the plasma. The Alfvén wing will thus lead Io in its orbit by a small and variable amount that depends on Io's plasma environment and the path length of the wave through the torus. The magnetic field perturbation resulting from this interaction was observed by the magnetic field experiment on Voyager 1 as it passed by the IFT, just south of Io's orbit, in March of 1979 (*7*). About 5×10^6 A of current flows in this circuit (*7, 8*), and nearly 2×10^{12} W of power is dissipated in the system (*7*).

In 33 of 204 infrared images of Jupiter at high spatial resolution, we identified a very localized and distinct emission feature that appears in association with Io's motion through the Jovian magnetosphere. These images were obtained at a wavelength of 3.40 μm with the ProtoCAM infrared camera and the National Aeronautics and Space Administration's (NASA's) 3-m Infrared Telescope Facility (IRTF) at the Mauna Kea Observatory. Such images are dominated by emission from H_3^+ originating well above the methane homopause in both polar regions (*9*). Methane is strongly absorbing at 3.40 μm and effectively masks emission from lower altitudes, including thermal emissions and sunlight reflected from clouds deeper in the atmosphere. Observations at this particular wavelength provide images of the distribution of H_3^+ with a relatively large effective signal-to-noise ratio (several hundreds). The molecular ion H_3^+ is formed at the base of the exosphere by impact ionization of molecular H_2 followed by conversion to H_3^+ through a rapid ion-molecule reaction ($H_2^+ + H_2 \rightarrow H_3^+ + H$).

Figure 1 shows a mosaic of nine 3.40-μm ProtoCAM images of Jupiter in which the H_3^+ aurora appears prominently. The relatively intense polar emissions appear in association with the "last closed field line," although some displacement of the model "auroral oval" is required to fit the observations. The auroral emissions are extensively limb-brightened and time-variable; a full account of the morphology of the Jovian auroras will appear elsewhere (*10*). Our interest is in the faint emission feature appearing near the foot of the (instantaneous) IFT, approximately 8° equatorward of the auroras and near the leftmost limb of the planet in both hemispheres (Fig. 1). This emission feature accounts for

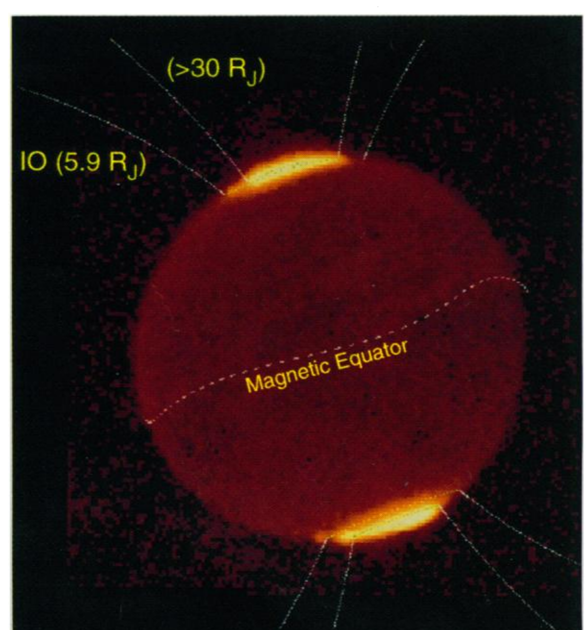

Fig. 1. Mosaic of nine ProtoCAM images of Jupiter (304° CML) at 3.40 μm on 12 January 1992 (*19*). The bright polar features are caused by H_3^+ emission occurring well above the methane homopause. A meridian plane projection of magnetic field lines originating beyond 30 R_J and at the orbital radial distance of Io (5.9 R_J) are superposed on the mosaic. These are computed using the O_6 planetary magnetic field model (*11*) combined with a magnetodisc model (*20*) that accounts for Jupiter's extensive ring currents. The leftmost field line is traced from the instantaneous position of Io at 79° Io phase. The vast majority of H_3^+ emission originates from the auroral oval approximated by the footprint of the last closed field line. The two faint emission features seen near the leftmost limb just equatorward of the aurora in both hemispheres are the surface expression of the electrodynamic interaction of the satellite Io with Jupiter's magnetosphere.

J. E. P. Connerney, Laboratory for Extraterrestrial Physics, NASA Goddard Space Flight Center, Greenbelt, MD 20771.
R. Baron, T. Satoh, T. Owen, Institute for Astronomy, University of Hawaii, Honolulu, HI.

less than 1% of the total integrated flux in either polar region. It can be seen near the limb in many mosaics for which the viewing geometry is favorable (Fig. 2), that is, those in which 45° ≤ Io phase ≤ 90° and 220° ≤ Io phase ≤ 270°. In this geometry, the foot of the IFT appears at its maximum separation from the much brighter auroral emission.

There are several sequences of mosaics in which the Io-associated emission feature can be observed coming into view over the dawn limb (Fig. 3) or disappearing from view over the dusk limb. The feature often appears over the dawn limb well in advance of the foot of the IFT computed with the O_6-model magnetic field, particularly in the northern hemisphere. The feature generally disappears from view at the dusk limb as the computed foot of the IFT passes over the limb. This cannot be explained by uncertainty of the longitude of the model Io foot (≈10°), which results from limited knowledge of the magnetic field (*11*).

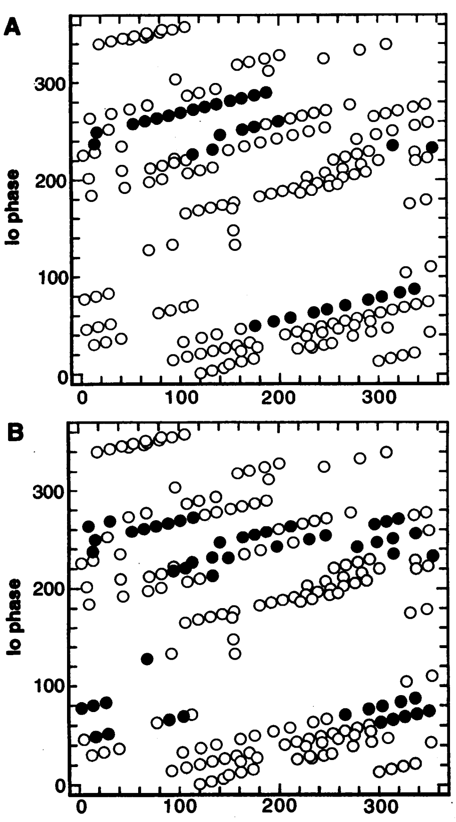

Fig. 2. Plot of Io phase and Jovian CML for all 3.40-μm mosaics of Jupiter acquired for both (**A**) north and (**B**) south hemispheres from 8 January through 18 April 1992 indicate mosaics in which the Io-associated feature appears as (solid circles) a distinct spot, (halftone) less distinct, or (open) not at all. The feature is evident in the south polar region at all CMLs, often seen whenever the viewing geometry is favorable (45° ≤ Io phase ≤ 90°, dawn limb; 220° ≤ Io phase ≤ 270°, dusk limb). In contrast, the feature has been identified in only a subset of north polar images, which would appear to provide favorable viewing geometry.

This emission occurs at high altitude and is visible at longitudes well beyond the limb of the planet, particularly in the northern hemisphere where it is observed close to the rotation pole (wide range of longitudes close to the limb). To obtain an accurate estimate of the feature's longitude with respect to the model foot, we concentrated on those few occasions when the feature was observed well inside of the limb of the planet.

One such mosaic of Jupiter (Fig. 4) has been processed to isolate the H_3^+ emission associated with the Io foot from that associated with the aurora. The IFT emission appears about 8° equatorward of the aurora and well inside the limb. The total integrated flux associated with the feature is ≈4.3×10^{-19} W cm^{-2} μm^{-1}, about 0.3 to 1.0% of the (variable) total flux from the aurora. The feature appears as a point source, perhaps slightly elongated along the path traced out by the foot of the IFT (Io footprint) by ≤5° longitude. This is consistent with the 10- to 1000-s lifetime of H_3^+ in the ionosphere (*12*). However, elongation of the emission feature along the Io footprint may also result from multiple reflection of the Alfvén wave between density gradients in the torus and in the ionosphere (*13*). Such multiply reflected Alfvén waves may account for the multiplicity of Jovian decametric arcs (*14*), a distinctive feature of high-frequency, Io-related radio emission.

In this example, the emission leads the (undisturbed) model field line footprint by $\Delta\phi \approx 15°$ in the direction of Io's orbital motion (in the downstream direction relative to motion of the magnetosphere past Io). Io's System III longitude at the time of observation was 120° λ_{III}, placing it nearly in the center of the high-density plasma torus. Four additional estimates of $\Delta\phi$, obtained from similar images of the south pole, ranged from 15° to 20° with no apparent correlation with Io's λ_{III}. The magnigude of $\Delta\phi$ is considerably larger than that expected ($\Delta\phi \approx 3°$) from Alfvén wave propagation (v_a = 400 km/s) through a path length of ≈1 R_J in the Io torus (*14*). A large $\Delta\phi$ favors the strongly coupled unipolar inductor model of the interaction (*4, 5*), controlled by the Pedersen conductivity of the Jovian ionosphere instead of the Alfvén conductance of the local plasma environment. This is also suggested by the apparent lack of detection of the emission feature at north polar longitudes (90° ≤ λ_{III} ≤ 240°) spanning the region of highest surface magnetic field strength (ionospheric Pedersen conductivity is approximately inversely proportional to magnetic field strength). As noted by Goldreich and Lynden-Bell (*5*), a 15° lead of the foot of the IFT with respect to that of the undisturbed field is exactly that required to symmetrize the observation of Jovian DAM at 90° and 240° Io phase, relative to an observer at 180° phase (Earth).

These observations establish an unambiguous reference on Jupiter's surface with which existing magnetic field models may be improved and with which other observations of polar phenomena may be organized. Current magnetic field models are derived from in situ observations obtained by spacecraft well above the planet's surface. Consequently, the field near the surface is less well constrained, leading to considerable uncertainty in the association of surface phenomena (for example, the aurorae) with distant magnetospheric source regions (*11*). The observations of the foot of the IFT that could be accurately located on the surface of the planet are shown in Fig. 5, A and B. These observa-

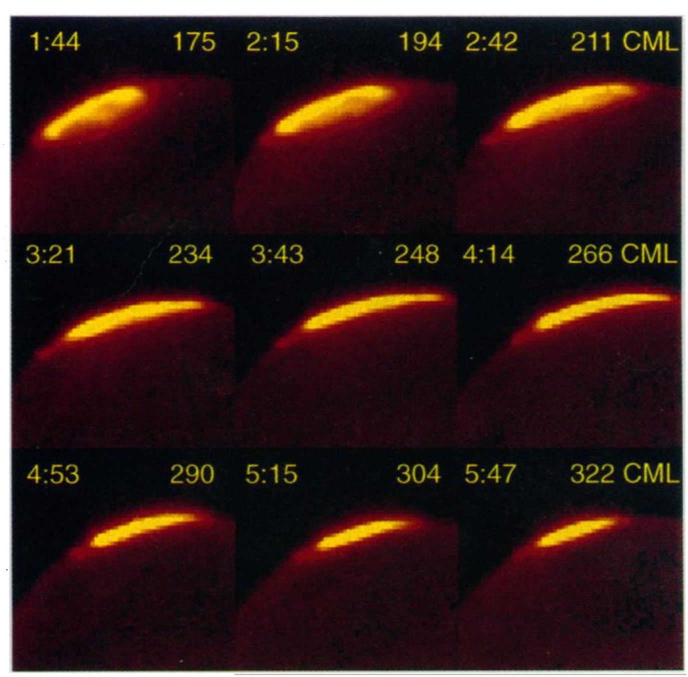

Fig. 3. Sequence of nine consecutive 3.40-μm images obtained on 12 January 1992. The Io-associated emission feature appears at the limb in the northern hemisphere, just equatorward of the aurora, in the second image, which was acquired at 2:15 HST and 194° CML. This feature was observed in all subsequent north polar images through the last image of this day (5:47 HST, 322° CML). It is not clearly visible near the southern limb (not shown) until 4:53 HST (290° CML). Io phase increases with time from 50° through 84°.

tions traced out the path followed by the foot of the IFT as Io moved through the Jovian magnetosphere. The latitude of the emission feature was determined to within 2°, but the longitude of the feature was difficult to estimate when it was observed near the limb. When the feature was observed well inside the limb (southern hemisphere), its longitude could be determined to within 3° to 5°.

The IFT footprint was located with greater accuracy than in existing models (*11*) and, when used as a constraint, may yield improved magnetic field models. A few immediate conclusions may be drawn from simple arguments based on conservation of flux. In the south, the model footprint appears shifted slightly with respect to the observations and is significantly larger, indicating that the model systematically underestimates the magnetic field magnitude in the south polar region by about 2 G. Thus, field magnitudes along the southern foot of the IFT range from about 10 to 12.6 G. This is sufficient to account for the maximum frequency of the Io C (35 MHz) and non-Io C (30 to 32 MHz) decameter radio sources, assuming emission occurs at the local electron gyrofrequency. This conclusion resolves a persistent objection to localization of this component of DAM in the south polar region (*2*).

The emission was not clearly identified in the north at longitudes between 90° and 240° λ_{III}, even though many images with the appropriate geometry were obtained. In this longitude range, the surface magnetic field strength is large, significantly in excess of that encountered at the conjugate point in the south polar region (*11*). This suggests that current may be preferentially conducted to and from Io toward the ionospheric foot characterized by the weaker magnetic field. The northern longitudes over which the H_3^+ emission feature was not observed correspond to those from which DAM is preferentially emitted. This anticorrelation suggests that DAM is generated by upward-propagating electrons that have been reflected back along the IFT toward Io in regions of high surface magnetic field strength (*15*).

Observations of the ultraviolet (UV) aurora have been obtained by the Voyager Ultraviolet Spectrometer (UVS) experiment (*16*), the Hubble Space Telescope (*17*), and the International Ultraviolet Explorer (IUE) satellite (*18*). Limited spatial resolution, longitude coverage, and the limited accuracy of magnetic field models has thus far hampered efforts to relate these UV emissions to the infrared aurora or to a particular source region in the Jovian magnetosphere. Our observations of the IFT in the north agree well with the location of the UV aurora seen by the UVS experiment (*16*), in the region of longitude coverage available. The IUE observations are well modeled by an emission source distributed along the foot of a flux tube just poleward of the model Io footprint (*18*). This is consistent with the UV emissions originating along the footprint of the IFT (Fig. 5B). The charged particles that excite these polar UV emissions originate at or just beyond Io's orbit (5.9 R_J), that is, in or near the Io plasma torus. The UV aurora occurs at all longitudes and extends equatorward of the infrared H_3^+ aurora. The latter emission, like the terrestrial aurora, occurs at high magnetic latitudes linked to the more distant reaches of the magnetosphere ($\gtrsim 30\ R_J$).

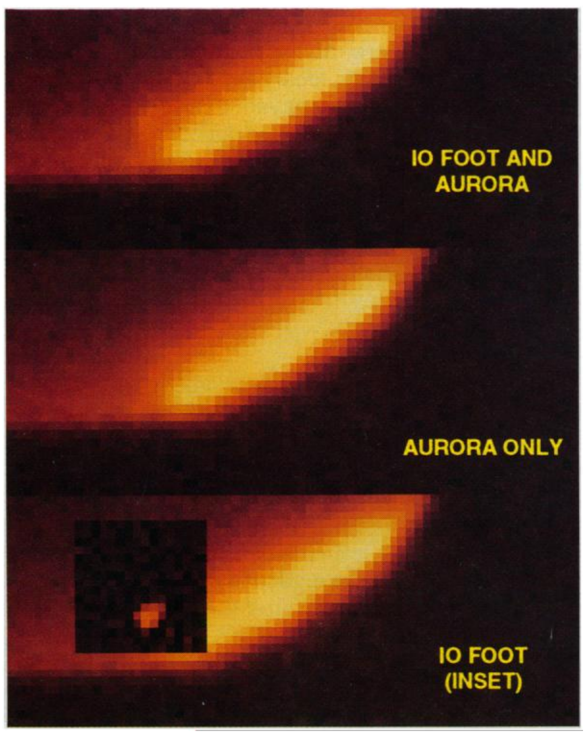

Fig. 4. A 3.40-μm image of the south polar region processed to isolate the Io-associated feature. The image was acquired at 3:24 HST on 30 January 1992 at 68° CML and 128° Io phase. In the upper image, the Io-associated feature is 8° to 10° equatorward of the aurora and well inside the limb. The center image shows emission from the aurora only, after the removal of the Io-associated feature. The bottom image shows a 16 pixel by 16 pixel inset (0.35–arc sec pixels) from which the background flux has been subtracted, leaving only H_3^+ emission associated with the Io foot. The feature appears like that of a point source, perhaps slightly elongated along the path of Io's L shell footprint. The longitude of the feature leads the footprint of the model field line by ~15° in the direction of Io's orbital motion (in the downstream direction relative to motion of the magnetosphere past Io).

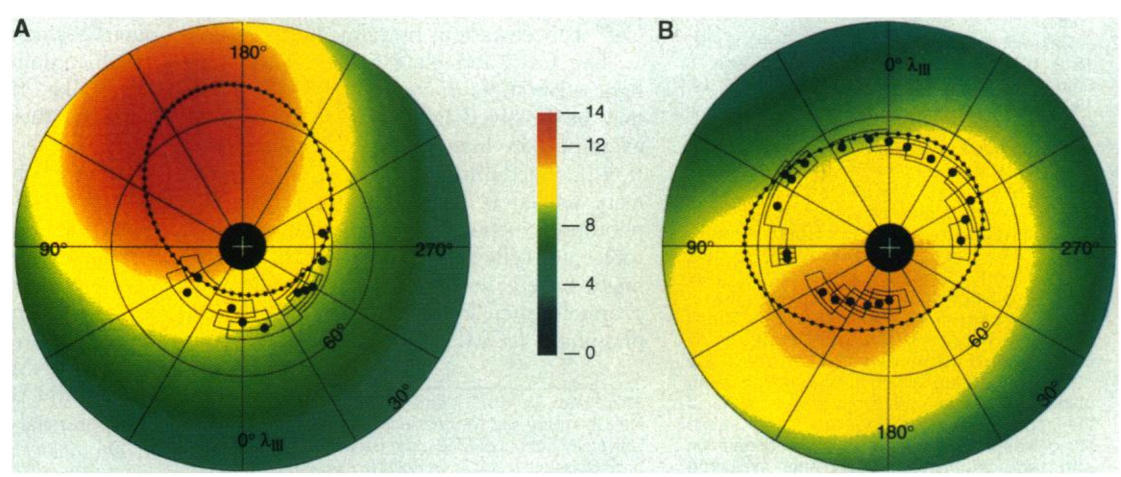

Fig. 5. Polar orthographic projection of the latitude and longitude of the distinct Io-associated features (large filled circles) and the estimated error of location for each observation (arc segments) for the (**A**) north and (**B**) south polar regions. The magnitude of the model magnetic field on the dynamically flattened (1/15.4) surface is indicated by color, with the greatest field strength (to 14 G) in red and weaker field magnitudes in yellow and green (~7 G). The footprint of the model IFT, computed with the O_6 magnetic field and current-sheet model (*11*), is indicated with the connected dots.

These observations provide direct evidence of the coupling between Io and the Jovian ionosphere, marking the (localized) impact of Io-accelerated charged particles in Jupiter's ionosphere. Further observations of the IFT foot may provide additional information regarding the interaction of Io and Jupiter's magnetosphere, the source location and generation of DAM, and Jupiter's magnetic field.

REFERENCES AND NOTES

1. B. F. Burke and K. L. Franklin, *J. Geophys. Res.* **60**, 213 (1955).
2. T. D. Carr, M. D. Desch, J. K. Alexander, in *Physics of the Jovian Magnetosphere*, A. Dessler, Ed. (Cambridge Univ. Press, Cambridge, 1983), pp. 1–50.
3. E. K. Bigg, *Nature* **203**, 1008 (1964).
4. J. H. Piddington and J. F. Drake, *ibid.* **217**, 935 (1968).
5. P. Goldreich and D. Lynden-Bell, *Astrophys. J.* **156**, 59 (1969).
6. The general description of this type of interaction, applied to the orbital decay of the Echo satellite, was given by S. D. Drell, H. M. Foley, and M. A. Ruderman [*J. Geophys. Res.* **70**, 3131 (1965)]; extension of this work and application to Io was done by F. M. Neubauer [*ibid.* **85**, 1171 (1980)], C. K. Goertz and P. A. Deift [*Planet. Space Sci.* **21**, 1399 (1973)], and C. K. Goertz [*J. Geophys. Res.* **85**, 2949 (1980)].
7. N. F. Ness *et al.*, *Science* **204**, 982 (1979).
8. M. H. Acuña, F. M. Neubauer, N. F. Ness, *J. Geophys. Res.* **86**, 8513 (1981); D. J. Southwood *et al.*, *ibid.* **85**, 5959 (1980).
9. R. L. Baron *et al.*, *Nature* **353**, 539 (1991); S. J. Kim *et al.*, *ibid.*, p. 536. The H_3^+ ion was first detected spectroscopically by P. Drossart *et al.* [*ibid.* **340**, 539 (1989)].
10. R. L. Baron *et al.*, *ibid.*, in press.
11. J. E. P. Connerney, in *Planetary Radio Emissions III*, H. Rucker, M. L. Kaiser, S. J. Bauer, Eds. (Austrian Academy of Sciences Press, Vienna, 1992), pp. 13–33; ______, M. H. Acuña, N. F. Ness, in preparation.
12. Y. H. Kim, J. Fox, H. S. Porter, *J. Geophys. Res.* **97**, 6093 (1992).
13. F. M. Neubauer, *ibid.* **85**, 1171 (1980).
14. D. A. Gurnett and C. K. Goertz, *ibid.* **86**, 717 (1981); Y. Leblanc and F. Bagenal, in *Planetary Radio Emissions II*, H. O. Rucker, S. J. Bauer, B. M. Pedersen, Eds. (University of Graz, Graz, Austria, 1988), pp. 127–138.
15. For a review of potential generation mechanisms for DAM, see M. L. Goldstein and C. K. Goertz, in (*2*), pp. 317–352.
16. A. L. Broadfoot *et al.*, *J. Geophys. Res.* **86**, 8259 (1981).
17. J. Caldwell, B. Turgeon, X.-M. Hua, *Science* **257**, 1512 (1992); V. Dols, J. C. Gérard, F. Paresce, R. Prangé, A. Vidal-Madjar, *Geophys. Res. Lett.* **19**, 1803 (1992); J. C. Gérard, V. Dols, F. Paresce, R. Prangé, *J. Geophys. Res.*, in press.
18. T. A. Livengood *et al.*, *Icarus* **97**, 26 (1992).
19. All mosaics were constructed by cross-correlation of the reduced (sky-subtracted, flattened, less bad pixels) 3.40-μm images, each of which was acquired with an effective integration time of 30 s and ~1% spectral resolution. Image smear attributable to Jupiter's rotation is negligible (Jupiter rotates by only 0.3° in longitude during each exposure). A full mosaic requires ~13 min of observation, during which Jupiter rotates by 8° longitude. Each mosaic is labeled with the central meridian longitude (CML) (in System III) of the center image, which may differ from that of the first or last image by no more than 4°. Limb fitting was accomplished by cross correlation with a limb-brightened model planet, excluding the bright polar region. A red leak correction was made with the use of a similar set of images at 4.9 μm acquired contemporaneously. Each pixel subtends 0.35 arc sec; tracking and positional errors introduced in construction of the mosaic are estimated to be subpixel in magnitude. Image times are Hawaii Standard Time (HST), related to Universal Time (UT) by UT = HST + 10 hours.
20. J. E. P. Connerney, M. H. Acuña, N. F. Ness, *J. Geophys. Res.* **86**, 8370 (1981).

21. We acknowledge the assistance of IRTF telescope operators D. Griep, C. Kaminski, and W. Golish and thank R. Joseph and the staff of the Institute for Astronomy at the University of Hawaii at Manoa. We acknowledge the assistance of J. Harrington, who was instrumental in the acquisition and processing of many of these images, and discussions with colleagues S. Miller, M. J. Mumma, T. J. Birmingham, and T. A. Livengood. Supported by the Yamada Science Foundation, Japan (T.S.). J.E.P.C. is a visiting astronomer at IRTF, which is operated by the University of Hawaii under contract to NASA.

8 June 1993; accepted 13 September 1993

Dependence of Calmodulin Localization in the Retina on the NINAC Unconventional Myosin

Jeffery A. Porter, Mujun Yu, Stephen K. Doberstein, Thomas D. Pollard, Craig Montell

Calmodulin is a highly conserved regulatory protein found in all eukaryotic organisms which mediates a variety of calcium ion–dependent signaling pathways. In the *Drosophila* retina, calmodulin was concentrated in the photoreceptor cell microvillar structure, the rhabdomere, and was found in lower amounts in the sub-rhabdomeral cytoplasm. This calmodulin localization was dependent on the NINAC (neither inactivation nor afterpotential C) unconventional myosins. Mutant flies lacking the rhabdomere-specific p174 NINAC protein did not concentrate calmodulin in the rhabdomere, whereas flies lacking the sub-rhabdomeral p132 isoform had no detectable cytoplasmic calmodulin. Furthermore, a defect in vision resulted when calmodulin was not concentrated in the rhabdomeres, suggesting a role for calmodulin in the regulation of fly phototransduction. A general function of unconventional myosins may be to control the subcellular distribution of calmodulin.

The intracellular Ca^{2+} receptor calmodulin is a primary mediator of Ca^{2+}-dependent signaling in most eukaryotic cells (*1*). It is among the most highly conserved proteins, differing between vertebrates and *Drosophila* in only 3 of 148 amino acids (*2*). Upon binding Ca^{2+}, calmodulin undergoes a conformational change rendering the protein competent to bind and alter the activities of target proteins (*1*). Thus, many proteins including protein kinases, protein phosphatases, ion channels, Ca^{2+} pumps, nitric oxide synthetase, inositol triphosphate kinase, and cyclic nucleotide phosphodiesterase are regulated by intracellular Ca^{2+} concentrations by calmodulin (*1*).

The Ca^{2+} ion plays a central role in light adaptation in vertebrate vision and may be involved in both adaptation and excitation in invertebrate phototransduction. Calmodulin could be one of the primary mediators of the Ca^{2+} response in phototransduction (*3*). Vertebrate rod photoreceptor cells contain calmodulin, which might have a direct role in modulating ion channels gated by guanosine 3′,5′-monophosphate (cGMP) (*4*). Ion channels required for invertebrate phototransduction may also be regulated by calmodulin. Calmodulin is present in the invertebrate microvillar rhabdomeres of photoreceptor cells in the crayfish, squid, and blowfly (*5*). Furthermore, *Drosophila* has a retinal-specific calmodulin binding protein, TRP-L, which has sequence similarity to the photoreceptor-specific putative Ca^{2+} channel, TRP (*6–8*).

The rhabdomere, the specialized microvillar structure of the invertebrate photoreceptor, contains rhodopsin and other important components in phototransduction and is functionally analogous to the outer segments of vertebrate rod cells, which contain calmodulin. In addition, the microvillar rhabdomeres are structurally similar to the calmodulin-rich brush border of vertebrate intestinal epithelial cells (*9*). Like the brush borders, rhabdomeres consist of highly ordered microvilli composed of actin filaments connected to the surrounding plasma membrane by radial links (*9*).

The major calmodulin binding protein in the intestinal microvilli is an unconventional myosin called the brush border myosin I (*10*). Abundant unconventional myosins, NINAC (neither inactivation nor afterpotential C) p132 and p174, are found in *Drosophila* photoreceptor cells and consist of a protein kinase domain joined to a region homologous to the myosin heavy

J. A. Porter, M. Yu, C. Montell, Departments of Biological Chemistry and Neuroscience, The Johns Hopkins University School of Medicine, Baltimore, MD 21205.
S. K. Doberstein and T. D. Pollard, Department of Cell Biology and Anatomy, The Johns Hopkins University School of Medicine, Baltimore, MD 21205.